Fall 2015

Detection and cancellation of sinusoidal fading power variation in wireless communication systems

Sushruth Sastry

Department:

DETECTION AND CANCELLATION OF SINUSOIDAL FADING POWER VARIATION IN WIRELESS COMMUNICATION SYSTEMS

by

SUSHRUTH SASTRY

A THESIS

Presented to the Graduate Faculty of the

MISSOURI UNIVERSITY OF SCIENCE AND TECHNOLOGY

In Partial Fulfillment of the Requirements for the Degree

MASTER OF SCIENCE

in

ELECTRICAL ENGINEERING

2015

Approved by

Dr. Kurt Kosbar, Advisor
Dr. Steven Grant
Dr. Randy Moss

ABSTRACT

Fading channel estimation in wireless communication systems depends on an expected model for fading and any assumptions made about the channel itself. The bit error rate (BER) performance of the communication system is affected by how closely these assumptions made in designing the estimation technique match the deployment environment. Any unforeseen disturbances or hindrances in the environment deteriorate the BER performance of the system when the estimation system is not designed to combat such disturbances. To deal with such unforeseen obstacles, additional mathematical models can be proposed to model such disturbances and then the estimation techniques can either be reinforced with modular systems which work with the proposed models, or be redesigned as a whole with the help of actual observed data of the disturbances. The current thesis deals with such a scenario where sinusoidal variation is expected in the received power in addition to fading. A mathematical model of such power variation is assumed and a modular scheme is proposed to detect and combat the sinusoidal variation. The proposed scheme is tested by employing it in a simulated Multiple Input Multiple Output (MIMO) wireless communication system which adopts Space Time Block Coding (STBC) techniques.

ACKNOWLEDGMENTS

I would like to thank Dr. Kurt Kosbar for being my adviser and guiding me in completing the current thesis. I would like to thank Dr. Yahong Rosa Zheng for verifying and helping consider various issues regarding my work with very less time. I would like to thank Dr. Steven Grant for agreeing to be on the thesis committee. I would like to thank Dr. Randy Moss for agreeing to be on the thesis committee on such short notice and helping me with the thesis document.

TABLE OF CONTENTS

Page

LIST OF ILLUSTRATIONS

Figure Page

LIST OF TABLES

1. INTRODUCTION

In communication systems, the received signal power varies due to multiple factors in the communication environment. The most fundamental power variation that can be observed is the attenuation of the received signal as the receiver moves farther away from the transmitter. This is usually known as path loss. In addition to this variation on spatial difference, received signal power can also vary in time due to multi-path propagation of electromagnetic waves, among other possible factors. This is known as fading. This phenomenon can be modeled as a linear time-invariant system in between the receiver and transmitter, referred to as the communication channel. If the modeled channel appears to be made of multiple coefficients, meaning that inter-symbol interference is present, it is known as a frequency-selective channel. On the contrary, if the channel appears to have a single coefficient, it is known as a frequency-flat fading channel [1] [2]. These channel coefficients vary in time causing the received signal power to vary in a seemingly random manner. If the average received signal power variation is cancelled due to path loss, the random variation in received signal power usually follows Rayleigh distribution [3]. Such fading is also called Rayleigh fading. The combination of path loss and fading can also be jointly modeled as Rayleigh-lognormal fading [4].

In this thesis, along with the path attenuation and fading, a sinusoidal variation is assumed in the received signal power. Causes for such variations, how they affect the communication system, and a possible modular method to deal with such variations are presented here. The cancellation of such sinusoidal variations or harmonics from a signal, which usually arise due to a regular noise source, is a topic of interest in many fields[5][6][7].

Figure 1.1 helps visualize these fading power envelopes. Figure 1.1a shows

Rayleigh fading envelope $h(t)$ with 10 Hz Doppler frequency, Figure 1.1b shows Rayleigh fading that has progressive path loss component, and Figure 1.1c shows Rayleigh fading with a sinusoidal power variation along with progressive path loss.

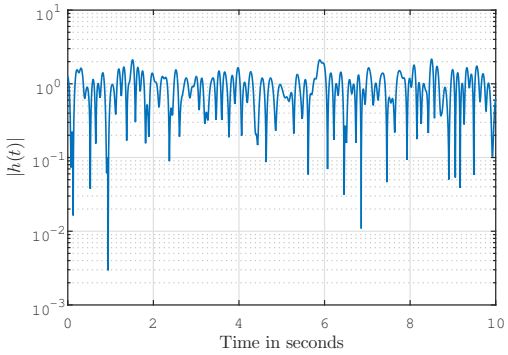

(a) Rayleigh fading

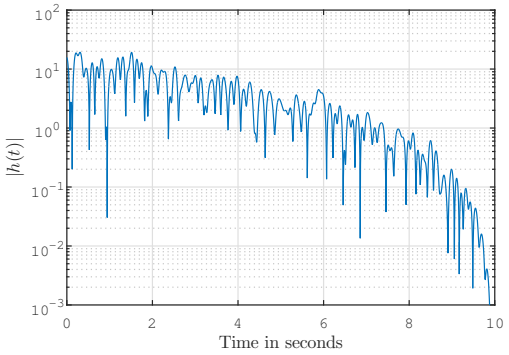

(b) Rayleigh fading with progressive path loss

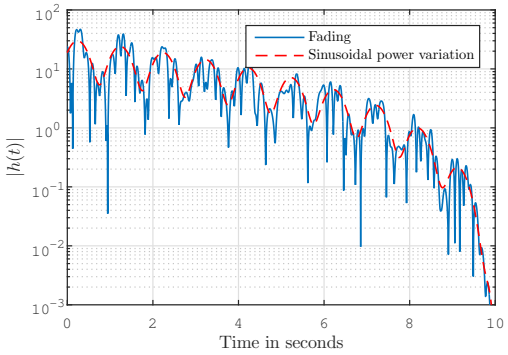

(c) Rayleigh fading with progressive path loss and sinusoidal power variation

Figure 1.1. Fading models

1.1. SCENARIO FOR APPLICATION

In a wireless communication system, sinusoidal variation in the received power can be a result of rotation in the antenna involved [8][9], movement of the receiver in

a diffraction pattern in the path of communication, or movement of objects creating changing diffraction patterns at the receiver [10].

Consider a wireless communication scenario, as depicted in Figure 1.2, showing two concyclic receiver antennae separated π radians apart on a circle with radius r, moving with a velocity v and rotating at δ Hz. The transmitter antenna shown is assumed to not be in motion.

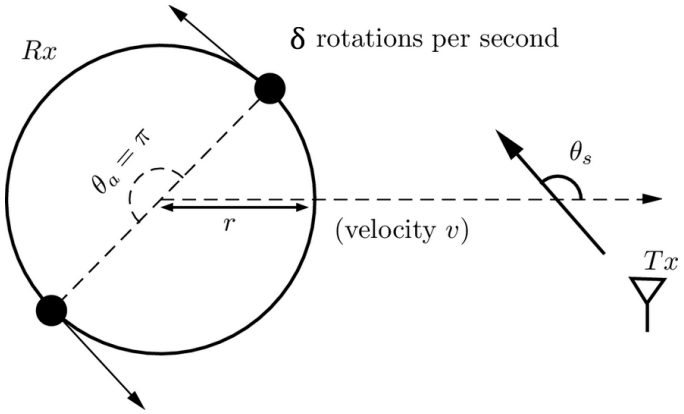

Figure 1.2. Wireless communication system scenario which can result in sinusoidal power variation at receiving end

Each of those receiver antennae produces a time-varying repetitive Doppler shift, which can be given by the equation 1.1.

$$f_d(t) = f_D \cos(\theta_s) + f_a(t) \tag{1.1}$$

Where θ_s is the angle of arrival of each path, f_D is the maximum doppler shift of fading, $f_a(t)$ is the time-varying part of the fading, and $f_d(t)$ is the resulting time-varying fading. Each path experiences different amount of shift.

It can be proved that $f_a(t)$ is given by equation 1.2 [11].

$$f_a(t) = \frac{2\pi\delta r}{\lambda} \sin\left[\theta_s - (2\pi\delta t + \theta_0)\right] \tag{1.2}$$

If the scenario/application can bear the following constraints:

1. The radius of the circle bearing the antennae is negligible compared to the distance between the transmitter and receiver.

2. The velocity of the receiver itself is much larger compared to the rotational velocity of the antennae (which depends on r and δ).

It can then be inferred that $f_a(t)$ is negligible compared to f_D and that such negligible changes in fading can be easily countered by channel estimation methods themselves intrinsically. Now the task purely becomes detecting and correcting the periodic change in the magnitude (due to line-of-sight (LOS) component in the fading) since that actually affects the performance of channel estimation schemes the most (as illustrated later).

The intent is to discuss the effects of such sinusoidal variation on the BER of the communication system and provide a method to detect and combat the same. The following sections of this chapter give an introduction to the concepts and configurations used in evaluating this scenario.

1.2. BASIC COMMUNICATION SYSTEM

A basic communication system is shown in Figure 1.3. The information from the binary source is modulated using digital modulation schemes. The modulated signal is transmitted using a transmitter antenna and travels through a communication medium (channel). The signal is then received by a receiver antenna. The signal

received is of the form shown in Equation 1.3 when represented in discrete time where k represents each bit index.

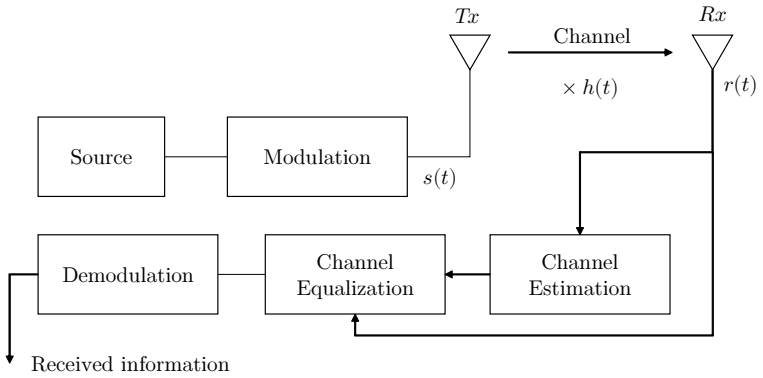

Figure 1.3. Simple wireless communication system

$$r(k) = s(k)h(k) + n(k) \tag{1.3}$$

At index k, where $s(k)$, $r(k)$, and $h(k)$ are discrete, complex baseband representations of signals represented in Figure 1.3, $n(k)$ is additive white Gaussian noise (AWGN) at the receiver antenna.

The received signal is then passed to a channel estimation block where the channel coefficient $h(k)$ is estimated and the channel effects are corrected in the channel equalization block. The equalized signal is then demodulated to receive an estimate of the transmitted information.

For the current experiment, BPSK modulation scheme was used for the communication system. For this implementation, quadrature signal representation [12] was used to represent the signal being transmitted (complex symbol +1 represents bit

1 while complex symbol -1 represents bit 0). Each symbol in the quadrature signal representation can be repeated multiple times consecutively so that each bit period consisted of multiple samples of the signal (denoted as samples per symbol or SPS). In this experiment, this option was kept at approximately 8.5 SPS to introduce timing error.

1.3. SIMULATING THE CHANNEL

The channel fading coefficient is calculated using a Rayleigh fading generator with correct statistical properties, as described in [13], given in Equation 1.4. In this implementation, frequency-flat fading is assumed [14].

$$Y(t) = Y_c(t) + jY_s(t) \tag{1.4}$$

$$Y_c(t) = \frac{1}{\sqrt{N}} \sum_{n=1}^{N} \cos(\omega_d \; t \;\; \cos \alpha_n \;\; + \;\; \phi_n) \tag{1.5}$$

$$Y_s(t) = \frac{1}{\sqrt{N}} \sum_{n=1}^{N} \sin(\omega_d \; t \;\; \cos \alpha_n \;\; + \;\; \phi_n) \tag{1.6}$$

$$\alpha_n = \frac{2\pi n \;\; + \;\; \theta_n}{\sqrt{N}}, \quad n = 0, 1, \cdots N \tag{1.7}$$

Where $j = \sqrt{-1}$, N is the number of fading paths, θ_n and ϕ_n are angles of incidence at the receiver assumed to be random and uniformly distributed over the interval $[-\pi, \pi)$, and ω_d is the Doppler angular frequency. A substitution of $h(k) = Y(kT_b)$ where T_b is the bit interval, allows the use of these equations to generate fading for the current implementation, provided the change in fading over the bit interval T_b is neglected.

1.4. CHANNEL ESTIMATION METHOD

A typical communication system works with blocks (or frames) of data with a particular structure that may include certain consistent (pattern of) symbols (called pilot symbols) at predefined locations (called pilot locations). The estimation method employed here [15] uses a pilot based, off-line trained, polynomial fitting process that generates an estimation matrix $\mathbf{H}$, which is used along with apparent fading calculated at pilot positions, to estimate the approximate fading envelope for the complete data frame.

The offline training method used to calculate a training matrix $\mathbf{H}$ requires separately generated fading envelopes for one frame of data and an AWGN corrupted version of the same at pilot positions. The function of this matrix $\mathbf{H}$ is to estimate the original fading vector $\mathbf{h}$ for the whole frame, given the corrupted fading vector (which contains observed fading only at pilot symbols) as given in Equation 1.8.

$$\hat{\mathbf{h}} = \mathbf{H}\mathbf{h}_k \tag{1.8}$$

The matrix $\mathbf{H}$ is calculated by generating Q ($= 1 \times 10^6$ frames for this simulation) number of fading vectors with F symbols in each frame and random fading parameters packed into a matrix $\mathbf{U}$. Where

$$\mathbf{U} = [\mathbf{h}_1\ \mathbf{h}_2\ \cdots\ \mathbf{h}_Q] \tag{1.9}$$

$$\mathbf{h}_i = [h_0\ h_1\ \cdots\ h_F]^T \quad where,\ i = 0,\ 1,\ \cdots\ Q \tag{1.10}$$

Another matrix $\hat{\mathbf{U}}$ is generated using each of the $\mathbf{h}$ vectors from Equation 1.9 corrupting them with varying levels of SNR (5dB to 20dB for this simulation), and selecting the fading coefficients at pilot positions as shown in equation 1.11.

$$\hat{\mathbf{U}} = [\mathbf{h}_{k,1}\ \mathbf{h}_{k,2}\ \cdots\ \mathbf{h}_{k,Q}] \tag{1.11}$$

$$\mathbf{h}_{k,i} = [h_{p1}\ h_{p2}\ \cdots\ h_{pP}]^T \tag{1.12}$$

where $p1, p2 \cdots pP$ are P pilot positions. Given the matrices $\mathbf{U}$ and $\hat{\mathbf{U}}$, the matrix $\mathbf{H}$ is calculated as given in 1.13.

$$\mathbf{H} = \mathbf{U}\hat{\mathbf{U}}^h \left(\mathbf{U}\hat{\mathbf{U}}^h\right)^{-1} \tag{1.13}$$

where $(\bullet)^h$ is the hermitian operation. Using the $\mathbf{H}$ matrix, the fading for the whole frame is calculated if the fading at pilot positions is known, which, in turn, is calculated as shown in 1.19.

For this simulation, 1×10^6 frames of fading were generated to populate $\mathbf{U}$ and $\hat{\mathbf{U}}$ as required. The value of ω_d was varied 5% from its mean of $2\pi 10$ radians/second uniformly.

1.5. SPACE TIME BLOCK CODING

To test the effects of sinusoidal variation in more advanced communication systems which provide redundancy through MIMO configurations, a basic STBC scheme proposed in [16] is simulated. The block diagram of this scheme is shown in Figure 1.4. Here, two transmitter antennae Tx_0 & Tx_1, and two receiver antennae Rx_0 and Rx_1 are used. The symbols are chosen to be transmitted in blocks called *frames*. The frame length is chosen so that frequency-flat fading is observed.

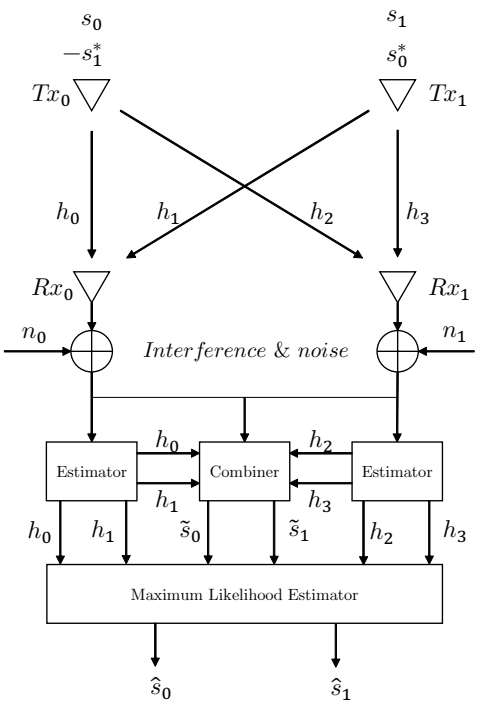

Figure 1.4. Alamouti STBC block diagram

As described in [16], a pair of symbols: s_0 and s_1, are transmitted using two bit intervals in each transmitter. First, the two symbols are transmitted simultaneously in the first bit interval, say index k, in each Tx. The next interval, indexed $k+1$, of each Tx is then used to transmit a modified version of the first symbol used on the other Tx as given in Table 1.1, where $(\cdot)^*$ denotes the complex conjugate operation.

Table 1.1. Transmission sequence for 2 × 2 MIMO system

	Symbol at Tx_0	Symbol at Tx_1
bit index k	s_0	s_1
bit index $k+1$	$-s_1^*$	s_0^*

The signals received at Rx_0 and Rx_1 can be represented mathematically as shown in Equation 1.14.

$$
\begin{aligned}
&at\ Rx_0-\\
&\qquad r_0 = r0(k) = h_0 s_0 + h_1 s_1 + n_0(k)\\
&\qquad r_1 = r0(k+1) = -h_0 s_1^* + h_1 s_0^* + n_0(k+1)\\
&at\ Rx_1-\\
&\qquad r_2 = r1(k) = h_2 s_0 + h_3 s_1 + n_1(k)\\
&\qquad r_3 = r1(k+1) = -h_2 s_1^* + h_3 s_0^* + n_1(k+1)
\end{aligned}
\tag{1.14}
$$

Where $r0(k)$ and $r1(k)$ are received signals through Rx_0 and Rx_1 respectively, n_0 and n_1 are noise signals at receiver antennas, and h_0 through h_3 are fading coefficients for all the four paths from each Tx to Rx as indicated in Figure 1.4, at index k.

An off-line trained channel estimator as proposed in [15] is used to proceed from this step of reception. Assuming that channel estimates $\hat{h}_0$ through $\hat{h}_3$ are available, the signals $r0$ through $r3$ are combined using equation 1.15.

$$\begin{aligned}\tilde{s}_0 &= h_0^* r_0 + h_1 r_1^* + h_2^* r_2 + h_3 r_3^* \\ \tilde{s}_1 &= h_1^* r_0 - h_0 r_1^* + h_3^* r_2 - h_2 r_3^*\end{aligned} \tag{1.15}$$

A maximum likelihood detector as defined in equation 1.16 is used to make an estimate of the transmitted symbols.

$$d^2(\tilde{s}_i, s_k) \leq d^2(\tilde{s}_i, s_k) \quad \forall\ i \neq k \tag{1.16}$$

where $d^2(\bullet)$ denotes the distance function which is given by equation 1.17

$$d^2(x, y) = (x - y)(x^* - y^*) \tag{1.17}$$

1.6. PILOT POSITIONING

The pilot system described in [15] is modified to best fit the STBC scheme used. The autocorrelation of Rayleigh fading is Bessel function of first order [13] ($= 2J_0(\omega_d \tau)$ where τ is the time delay) and thus has at least as many zero crossings as a cosine function of angular frequency ω_d [17]. This observation may suggest that the fading envelope for the frame can be expected to change significantly only if the time interval of each frame is greater than or about $\frac{\pi}{\omega_d}$. Thus, for this experiment, a single frame of data was assumed to span the time interval $\frac{\pi}{\omega_d}$. In such a frame structure, pilots are always placed in the same positions for both frames but as conjugates of their counterparts. An example is given in Equation 1.18.

$$\mathbf{s}_0 = [s_1\ s_2\ \cdots\ s_{i-1}\ p_i\ p_{i+1}\ s_{i+2}\ \cdots\ s_F] \tag{1.18}$$

where s_i is a symbol at position i, p_i is a pilot at position i and the frame consists of F symbols in total. All pilots are selected to be the value 1. This helps

estimate the fading at pilot positions, as shown in Equation 1.19.

$$\begin{aligned}
\mathbf{h}_{k0} &= \frac{\mathbf{r}_{0p} - \mathbf{r}_{1p}}{2} \\
\mathbf{h}_{k1} &= \frac{\mathbf{r}_{0p} + \mathbf{r}_{1p}}{2} \\
\mathbf{h}_{k2} &= \frac{\mathbf{r}_{2p} - \mathbf{r}_{3p}}{2} \\
\mathbf{h}_{k3} &= \frac{\mathbf{r}_{2p} + \mathbf{r}_{3p}}{2}
\end{aligned} \tag{1.19}$$

Where $\mathbf{h}_{k0}$ through $\mathbf{h}_{k3}$ are frames of fading coefficients at pilot symbols and $\mathbf{r}_{0p}$ through $\mathbf{r}_{3p}$ are received signal vectors sampled at pilot positions for each antenna.

The pilots are positioned based on requirements of each individual implementations as desired.

1.7. OVERVIEW OF THE SIGNALS IN THE SYSTEM

The following figures provide visual representation of the signals being transmitted at various stages of communication. Figure 1.5 shows the signal $s(k)$, which is completely real since it is a BPSK signal.

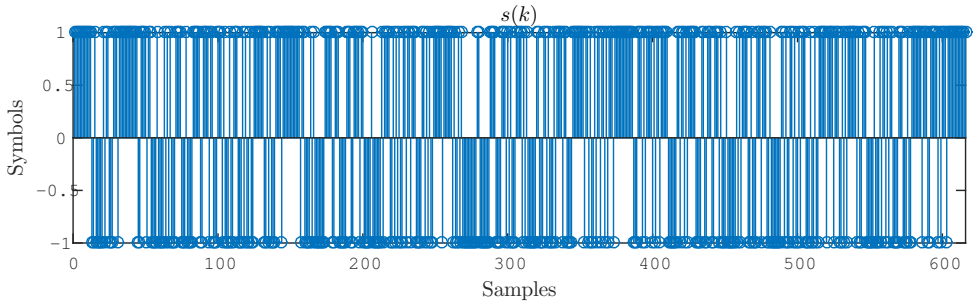

Figure 1.5. A frame of symbols to be transmitted

Figure 1.6 shows the STBC signals, which are $s_0(k)$ and $s_1(k)$, at both the transmitters Tx_0 and Tx_1. It also shows the pilot symbol locations. For the sake of simplicity, all pilot symbols are set to a level of +1 (bit 1).

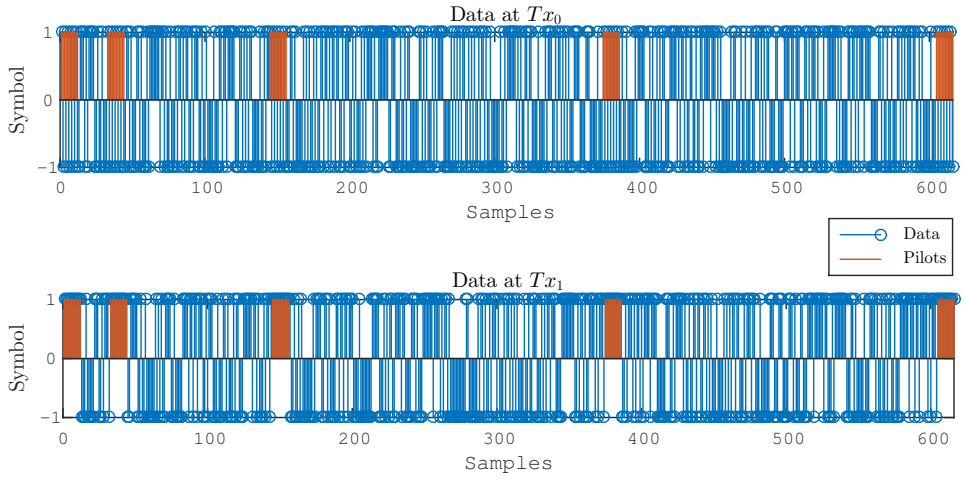

Figure 1.6. Multiplexed data according to Alamouti STBC

Figure 1.7 shows the fading envelopes of all four possible fading paths in the 2 x 2 Alamouti STBC system. It can be noted that the sinusoidal variation affects all four paths equally.

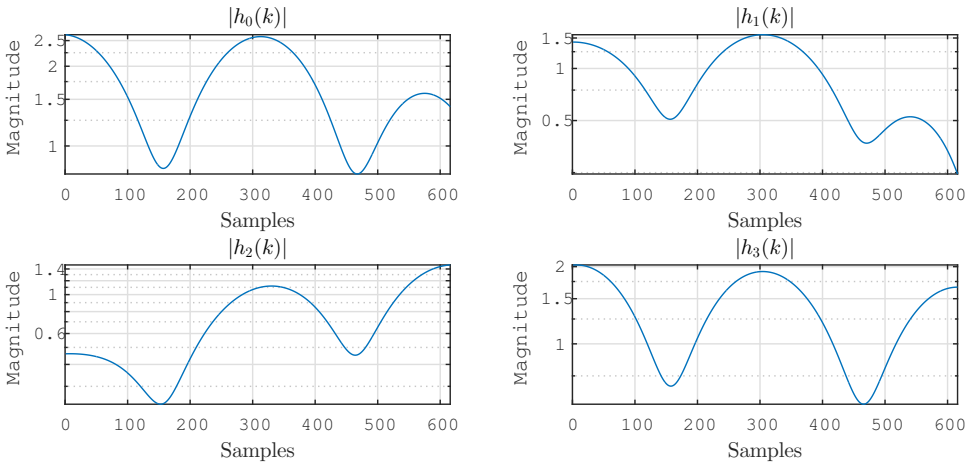

Figure 1.7. Fading envelopes for all fading paths

The signals received at both the receivers are shown in Figure 1.8. The system was simulated at SNR = 0dB for this reception to observe the system at its worst.

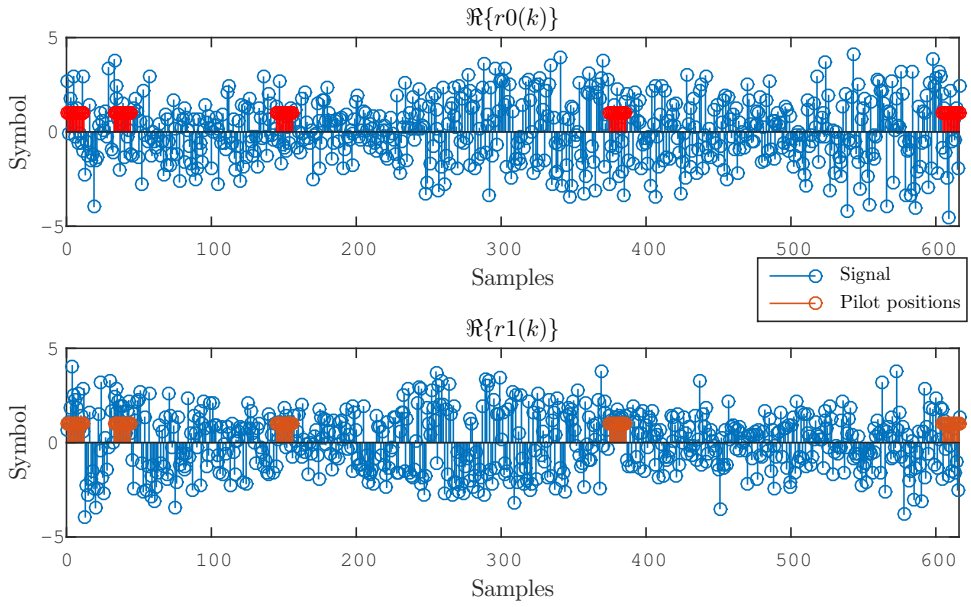

Figure 1.8. The received signal at Rx_0 and Rx_1

Figure 1.9 shows the demultiplexed signals according to Equation 1.19. It also shows the pilot symbols when they are demultiplexed, which demonstrates how the pilots are placed such that they are not scrambled with symbols when using the STBC scheme.

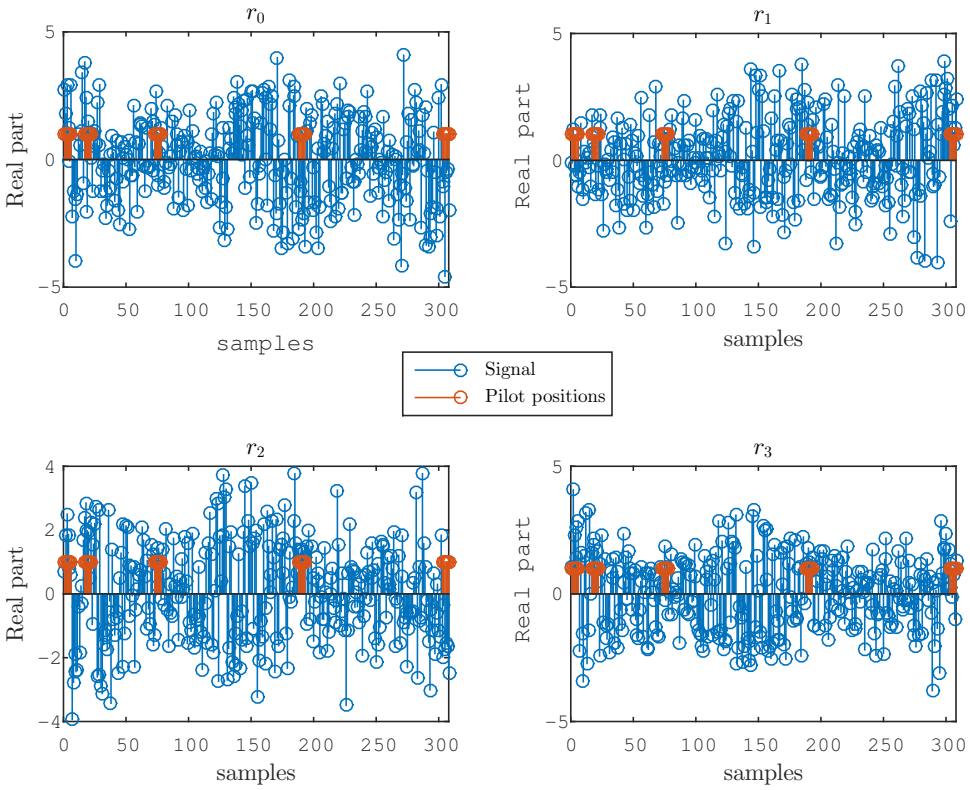

Figure 1.9. The signals r_0 through r_3 as given in equation 1.19

The channel estimation scheme does not contain information about any expected sinusoidal variation in the observed fading. Though the estimator is provided with calculated fading at pilot positions according to Equation 1.19, output of the estimator still suffers as illustrated by Figure 1.10.

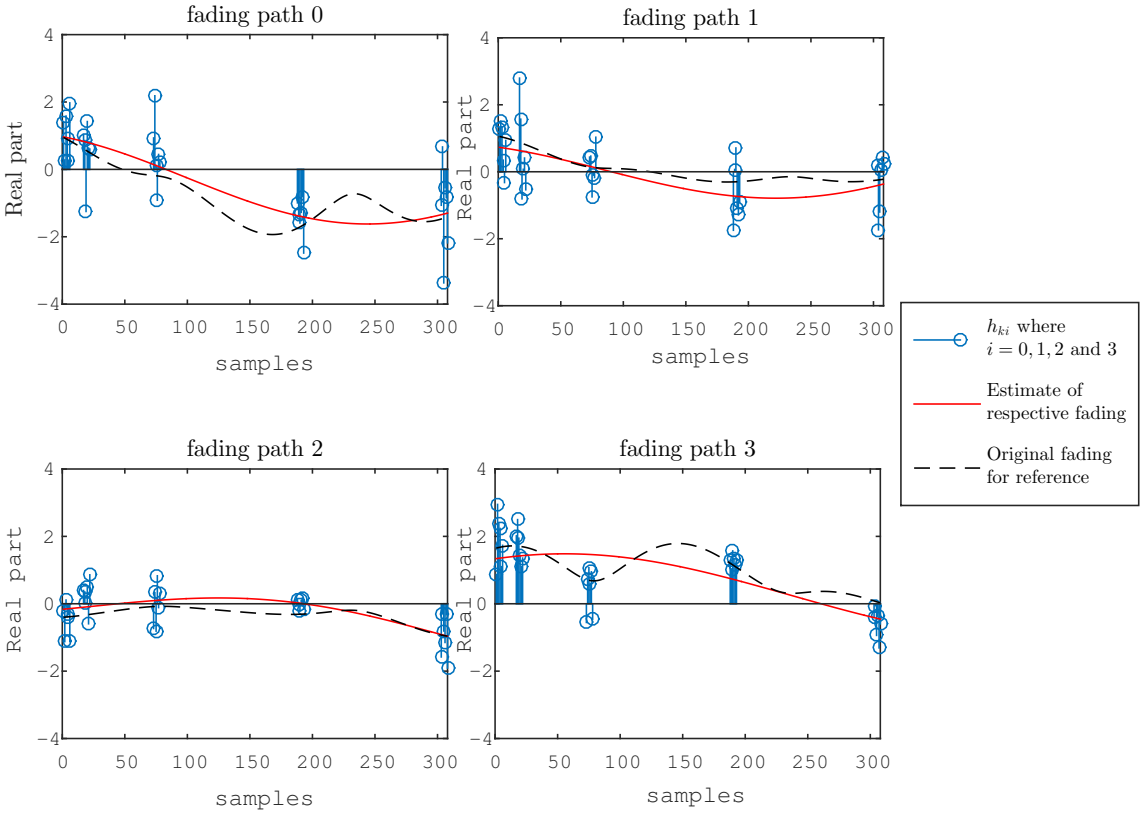

Figure 1.10. Observed fading at pilot positions and their estimates

The output of the combiner which uses signals r_0 through r_3, is shown in Figure 1.11. The same figure also shows the output of the ML detector compared with the original data.

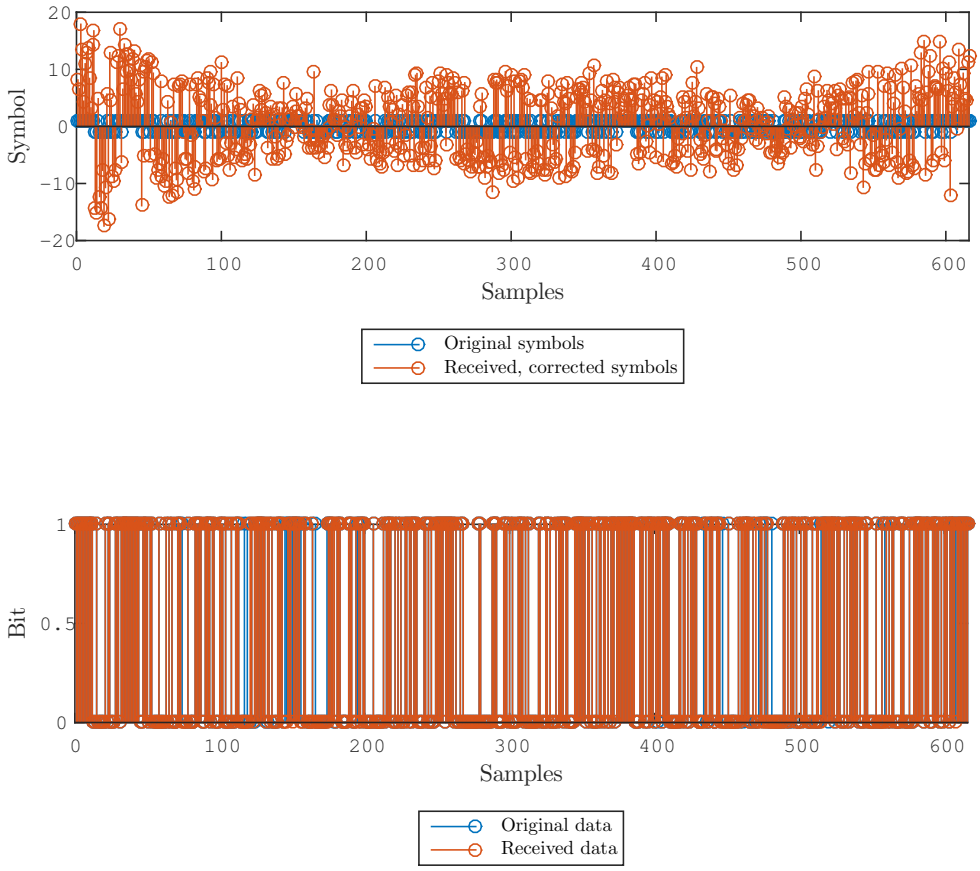

Figure 1.11. Observed fading at pilot positions and their estimates

2. SIMULATION AND OBSERVATIONS

The communication system described earlier was simulated and BER was used as a metric to evaluate the system. A logarithmic plot of error rate for corresponding SNR values, referred here as 'BER curve', is given in Figure 2.1. The given BER curve for perfect channel estimation matches the results provided in [16] closely (Data 2).

Figure 2.1 shows additional results: Data 1 shows the BER curve of the same system simulated under different conditions: where the Doppler frequency used to generate fading in transmission is slightly different (± 2 Hz uniformly random and centered at 13 Hz) from the actual Doppler frequency used in off-line training (10 Hz). This shows the effects of mismatch between the trained environment of the channel estimator and the actual environment of the wireless communication system employing it.

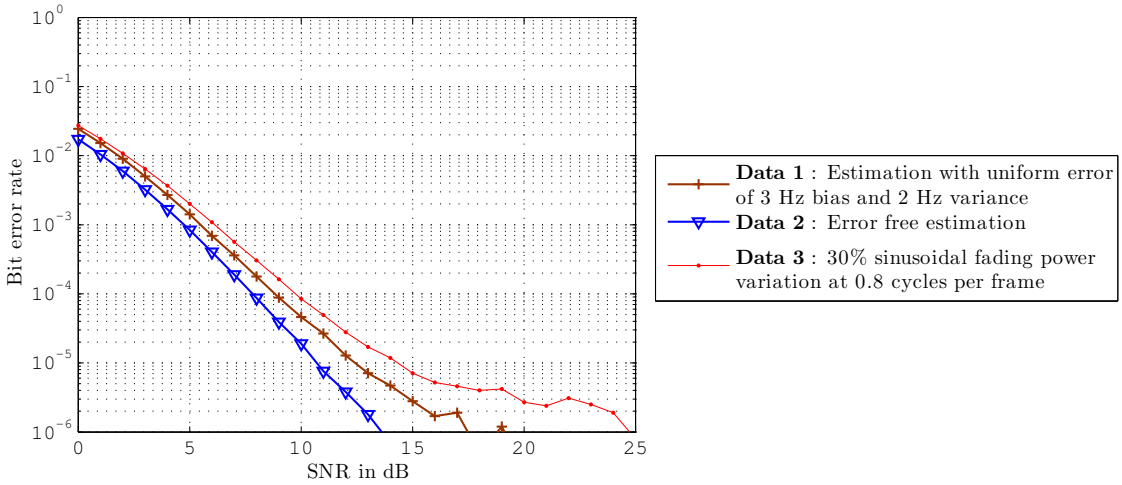

Figure 2.1. BER curves of the communication system being discussed

In Figure 2.1, Data 3 shows the effect of having the above-mentioned mismatch with a sinusoidal power variation in the fading. For demonstration purposes, the following conditions were used:

- The time interval of each frame was selected to be $T_f = \frac{\pi}{\omega_d}$ to match the correlation time as described earlier.

- The sinusoidal variation for fading power was generated to be centered at a power level of 0.5 [16] with an amplitude corresponding to 30% variation in power, a random initial phase angle, and a frequency corresponding to 0.8 cycles per frame. The frequency of sinusoidal variation is represented as 'cycles per frame' (CPF) so that its relation to the Doppler frequency of fading is relatively kept the same irrespective of actual frame time or the wireless carrier frequency used.

- The equation used to introduce the power variation is as given in Equation 2.1, where a is the DC level of the variation, C is the amplitude of the variation, f is the frequency in Hz, and ψ is a random initial phase angle.

$$\begin{aligned} h(k) &= \sqrt{a + Csin(\Theta)} \times Y(kT_b)), \\ \Theta &= 2\pi\delta kT_b + \psi \end{aligned} \tag{2.1}$$

To further examine the effects of frequency and amplitude of the sinusoidal variation, the simulation was run for different percentages of amplitude (from 10% to 80% fading power) and different frequencies of the sinusoid (from 0 to 4 CPF). The results are shown in Figure 2.2.

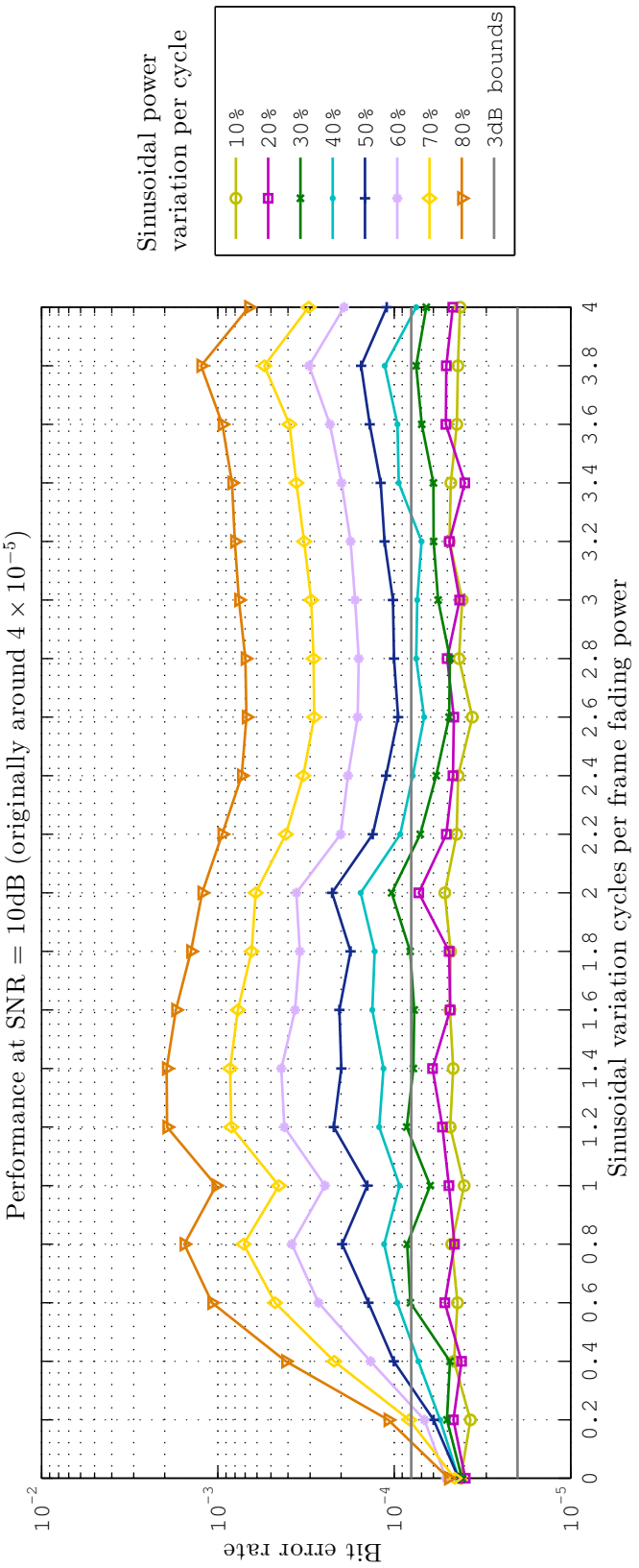

Figure 2.2. BER performance of the communication system at SNR of 10dB. The ±3 dB boundaries also indicated.

It is evident from Figure 2.2 that introducing a sinusoidal power variation with 50% variation in power and at 0.2 CPF to the fading can reduce the current system's BER performance by approximately 4 dB while operating at an SNR of 10dB.

3. EXISTING METHODOLOGIES AND APPLICABILITY

The problem of cancelling one or more sinusoidal disturbances is common in signal processing. Different applications call for different types of solutions based on the specifics of the system setup in each application. The signal setup of the current application requires cancelling out a sinusoidal variation in the received signal. Existing methodologies for cancelling a sinusoidal variation are listed below.

3.1. HARMONIC CANCELLATION TECHNIQUES

In the area of control engineering, regular patterns of machine interference are a common source of disturbance [18]. A number of harmonics cancellation methods are proposed in this matter [19, 20, 21]. Unknown harmonic noise signals in working plants are a significant source of disturbance that need to be addressed. The internal model principle states that in order to cancel an input, a system capable of producing the same is required [22].

The availability of such a system depends on estimating the frequency of disturbance and building a filtering system that gets rid of that particular frequency or a band of frequencies nearby. For applications in control engineering, such disturbances are usually from another part in the same plant and hence their frequencies can be easily identified. These control systems are mostly developed to counter sinusoidal interferences of known frequencies.

Although adaptive harmonic control methods already exist, they depend on a filter to remove the sinusoidal interference and calculate an error signal. Further adaptation is based on the error signal. These algorithms are still not applicable since the error signal in this scenario will contain more than just the desired signal and

interference, such as the Rayleigh fading envelope.

3.2. ADAPTIVE FILTERING TECHNIQUES

Adaptive filters are used to estimate unknown systems. Adaptive filters work on an input signal and its corresponding output signal from an unknown system. A typical adaptive filter system works on repetitively refining a randomly generated system (estimated system) to eventually reach the coefficients of the unknown system thus reducing the error between the output of the estimated system and the unknown system. An example of this is the least mean squared (LMS) algorithm, which works as shown in the block diagram in Figure 3.1.

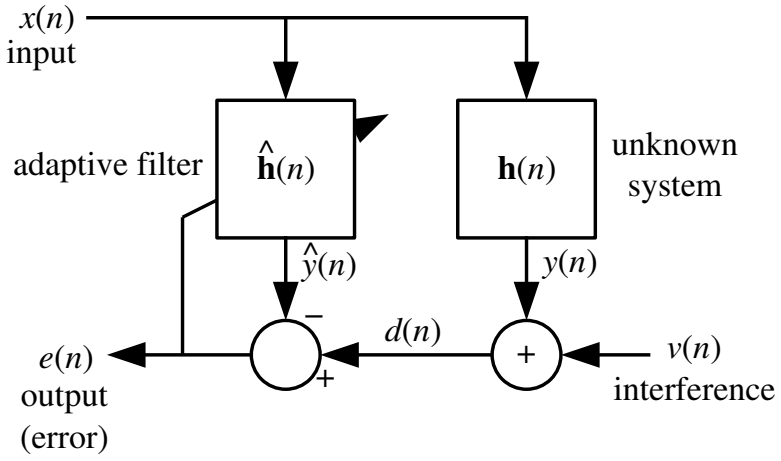

Figure 3.1. LMS adaptive filter block diagram

The system $\hat{\mathbf{h}}$ is assumed to be of N taps, and the whole vector of taps $\hat{\mathbf{h}}$ is jointly updated in a single update equation at iteration n, as given in Equation 3.1.

$$\hat{\mathbf{h}}(n+1) = \hat{\mathbf{h}}(n) + \mu \mathbf{x}(n) e^*(n) \tag{3.1}$$

where $\mathbf{x}(n)$ is a set of N input samples from index n to $n - N + 1$, and $e^*(n)$ is the approximate error signal as shown in Figure 3.1.

Adaptive algorithms can also be modified to cancel a single frequency by extracting that particular frequency from the output and generating the error signal. The update equation 3.1 does not support the current condition of having a high frequency BPSK modulated signal multiplied with a Rayleigh fading complex envelope and then multiplied with a sinusoidal power variation signal. Thus, the error signal generated in adaptive filtering systems cannot let the signal converge as the Rayleigh fading envelope has a high probability of having magnitudes about unity when normalized at the receiver.

3.3. AMPLITUDE MODULATION APPROACH

Since the sinusoidal fading power variation is multiplicative in nature, it can be viewed as an amplitude modulation problem. The spectral components of a typical received signal are shown in Figure 3.2.

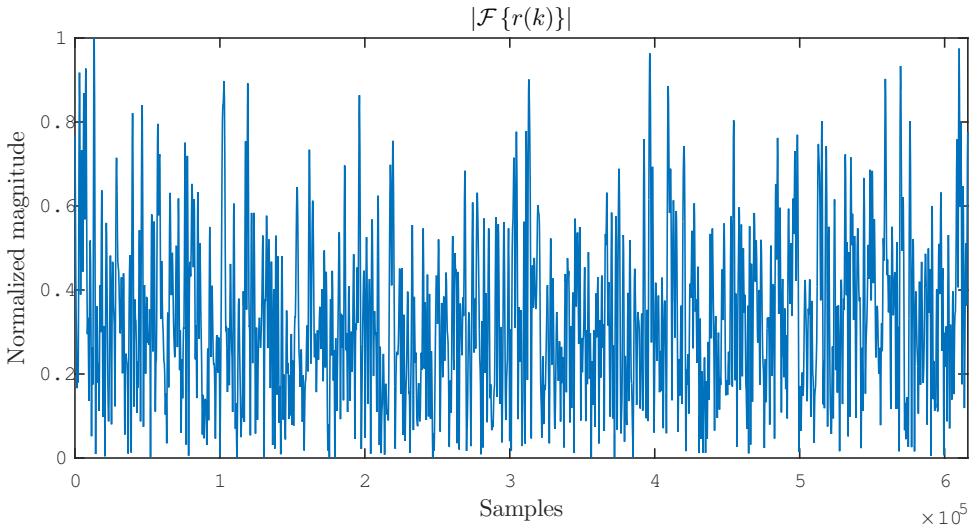

Figure 3.2. Spectral components of the received signal

The Figure 3.2 shows that the received signal is rich in spectral components. It is not possible to demodulate any sinusoidal power variation due to the sinusoidal variations of comparatively lower frequency.

3.4. GENERAL OBSERVATION

Though the received signal has many components over the whole of the frequency spectrum, the power of the received signal is expected to be consistent in a wireless communication system. Due to the Rayleigh fading and AWGN, the spectrum is expected to have a doppler power spectrum and noise, as shown in Figure 3.3.

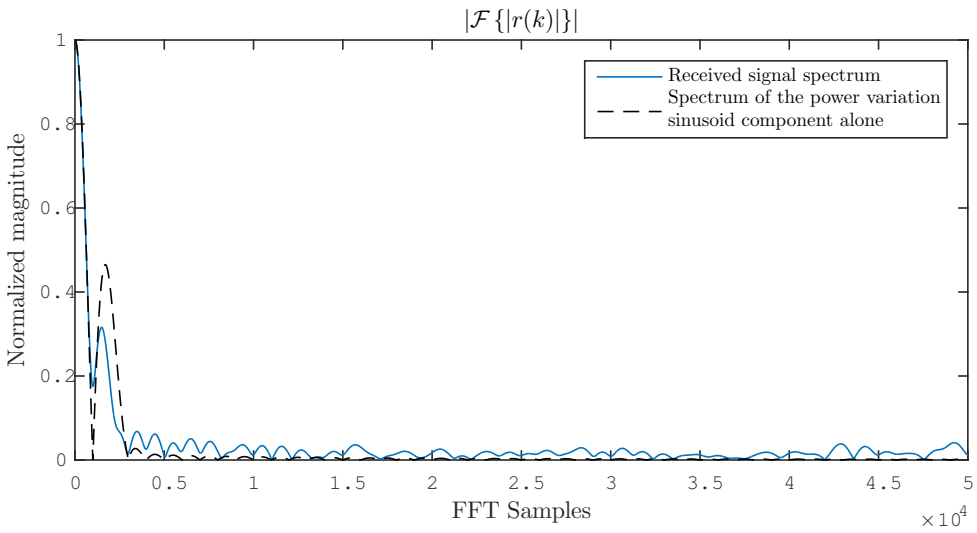

Figure 3.3. Frequency spectrum of the amplitude of the received signal with a sinusoidal power variation of 80% fading variation and 3 cpf frequency

It is possible to use $|r(k)|$ as a base signal for aforementioned mentioned methods since the sinusoidal component is readily visible. It must be noted that the aforementioned systems rely on an error signal that is expected to reduce as the disturbance is removed. However, the error in current scenario cannot be calculated until the channel effects are nullified and the channel estimator output is obtained. Which makes it impossible to use with above mentioned systems.

3.5. DIRECTION FOR SOLUTION

The sinusoidal variation can be observed in the frequency spectrum of received power. The sinusoidal variation can be extracted from the received signal and then used for cancellation.

3.6. REVIEW OF FREQUENCY DETECTION METHODS

Frequency detection methods are also known as pitch detection methods in the area of audio signal processing. Many methods are available for pitch detection in music-like audio signals [23]. A broad categorization of such methods can be listed as:

- Time domain methods
- Frequency domain methods
- Artificial intelligence (AI) methods

Some time domain methods depend on zero-crossing detection, which is not possible for the current scenario since the received power is always positive. Other time domain methods involve autocorrelation, which also cannot be used due to the autocorrelation properties of Rayleigh fading channel. For the sake of simplicity, AI methods are not considered for this implementation.

Since the received signal power has a Doppler frequency spectrum, frequency domain methods can be more effective in detecting sinusoids of higher frequency than the Doppler frequency of observed fading. Hence, frequency domain analysis can be chosen for detection of the sinusoidal variation. There are many frequency domain detection systems such as PMUSIC algorithm [24] and ESPRIT algorithm [25], that perform subspace analysis on the correlation matrix of the signal to be analyzed.

The MUSIC method is implemented using Matlab's inbuilt function `pmusic` [26] (please refer to the citation for mathematical equations). This method can be used when a number of expected fundamental frequencies in the signal to be analyzed is known since it uses the same number of highest eigenvalues of the correlation matrix of the signal to be analyzed when performing the analysis. The Figure 3.4 shows the

result of applying this algorithm onto the received signal power when 2, 4, and 8 fundamental frequencies are expected respectively.

The sinusoidal variation is almost invisible, and either the DC level of the received signal power or the noise is dominating instead of the sinusoidal variation. When the frequency of sinusoidal variation is comparable with the Doppler frequency, this method fails to detect the sinusoidal variation frequency and may give false-positives in the high frequency range.

Further analysis of the ESPRIT algorithm would lead to similar results since it is similar to MUSIC in terms of subspace technique but different in the way that it tries to suppress noise instead of enhancing required signals [27].

Thus, it is not conclusive to select a frequency detection system for general usage. It is advisable to select specific applicable frequency detection systems for specific implements of wireless communication systems. The method used in this implementation is based on fast Fourier transform (FFT), which is most widely used for simple frequency analysis and computationally more efficient than the previously discussed methods.

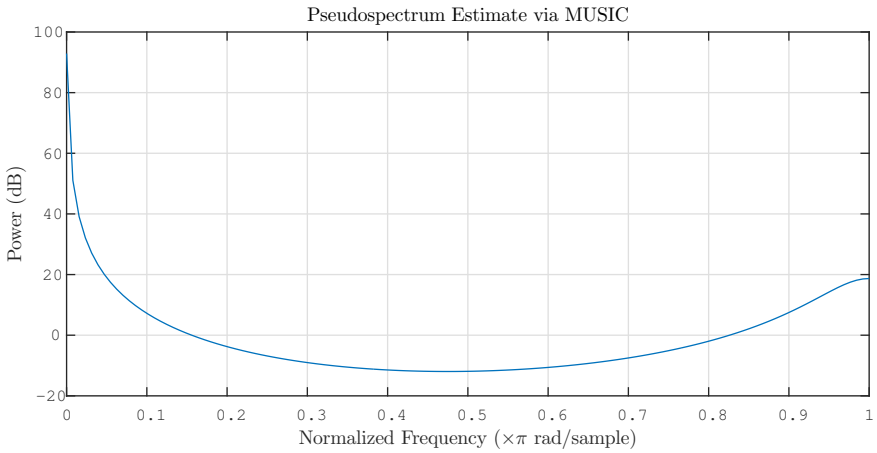

(a) MUSIC algorithm with 2 expected frequencies

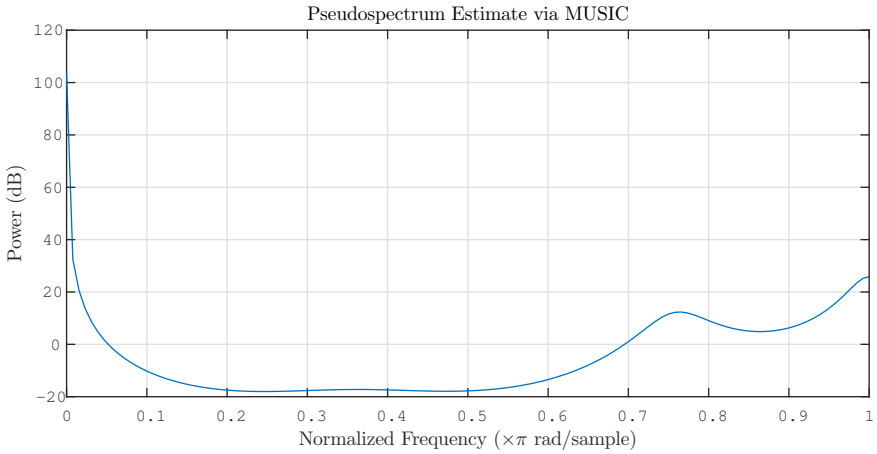

(b) MUSIC algorithm with 4 expected frequencies

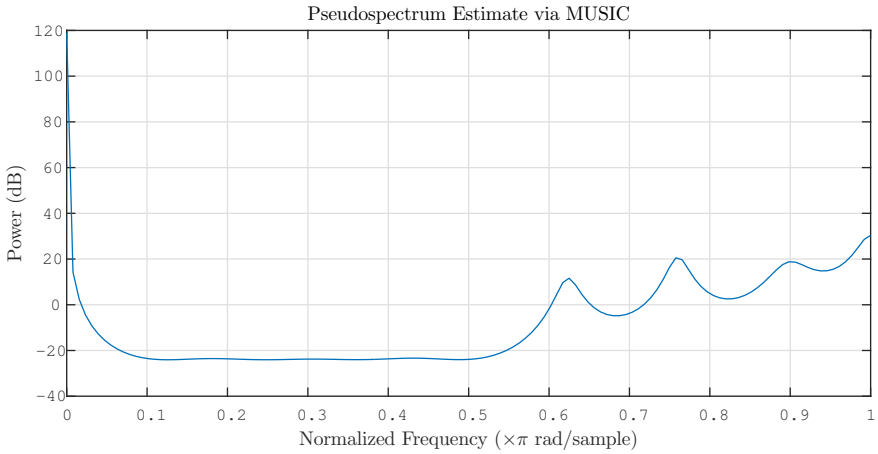

(c) MUSIC algorithm with 8 expected frequencies

Figure 3.4. Output of MUSIC algorithm

4. DETECTION AND CORRECTION OF THE SINUSOID

A readiness to combat the effects of a sinusoid with a frequency corresponding to ≥ 0.2 CPF enables tackling most of the errors shown in Figure 2.2, outside a 3dB boundary from the original BER. At least one cycle of the frequency (five frames of data) must be available to effectively measure the frequency of the fading using fast Fourier transform.

To detect the signal, consider the magnitude of the stored received signal $|p(k)|$ given by Equation 4.1, derived by taking magnitude of received signal $r(k)$, where $r(k) = r0(k) + r1(k)$. This preserves the sinusoidal variation since it is common for all channels and does not worsen the effects of fading in the received signal since all the fading paths are considered to be uncorrelated. This equation is the result of the fact that all symbols in PSK modulation have equal magnitude and are equal to unity.

$$|p(k)| = (a + Csin(\Theta))\,|r(k)| \tag{4.1}$$

Where $|r(k)|$ corresponds to the rest of the signal lumped together consisting of fading and noise. From here on, suitable frequency domain methods can be employed to detect the sinusoid based on the requirements and/or limitations of any implementation at hand. The next section outlines a method used in this implementation.

4.1. RECEIVED SIGNAL SPECTRUM

The fact that signals received in wireless communications have a Doppler power spectrum [28] [29] allows easy detection of the sinusoidal variation of higher

frequencies relative to ω_d. For variations of low frequency, a chirp-z-transform can be employed to observe the frequency spectrum of the received signal within certain frequency bounds, say 0 Hz to ω_d in Hz, in detail [30] (Stage 1). In this implementation, the frequency spectrum of Stage 1 is also multiplied with a rising function ($\sqrt[3]{ramp(f)}$) where $ramp(f)$ is a linear function increasing from 0 to 1 over the spectral frequency interval) to reject DC and dampen lower frequency signals. The rest of the frequency spectrum (until $F_s/2$, where $F_s = 1/T_b$) is calculated and used without the ramp function (Stage 2).

Figure 4.1 shows the normalized spectral components of 20 frames of received signal with a sinusoidal variation of 36.2545 CPF ($= \frac{36.2545\ \omega_d}{2\pi} \simeq 362.54Hz$) and 30% fading power variation for $T_b = 1.6276 \times 10^{-4}$ seconds.

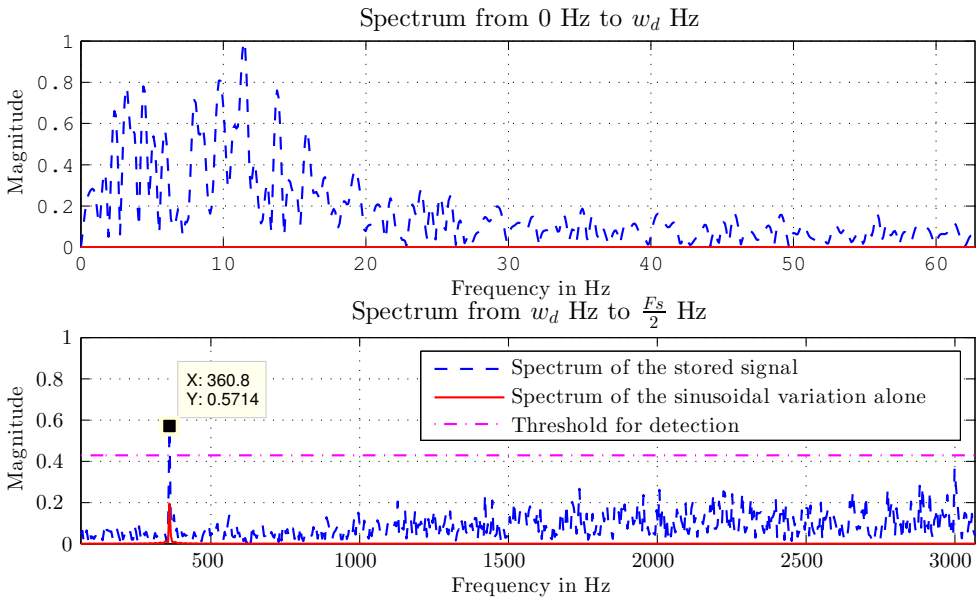

Figure 4.1. Spectral components of received signal and the sinusoidal variation compared, along with threshold. Stage 1 on top and Stage 2 on the bottom

4.2. SIMPLE FREQUENCY DETECTION

The threshold for the sinusoid detection was set at 75% of the maximum magnitude in Stage 2. Since the current problem is to reject a single sinusoid, a sinusoid is detected only when a single peak satisfies this threshold criterion. The sinusoid is assumed to be in this range and the frequency of this single peak is assumed to correspond to the frequency of the sinusoid. Otherwise, the frequency corresponding to the largest peak in Stage 1 is assumed to be the frequency of the sinusoid. This setup is prescribed only as a simple solution to facilitate the evaluation of systems performance when the frequency of the sinusoid is known.

4.3. CANCELLING THE EFFECTS OF THE SINUSOID

Once the frequency is estimated, an ideal single frequency pass filter designed at this frequency is used to construct the correction signal $p_c(k)$ as given in Equation 4.2.

$$\begin{aligned} e(k) &= \mathcal{F}^{-1}\left\{\mathcal{F}\left\{|p(k)|\right\} * H_f\right\} \\ p_c(k) &= \sqrt{2} * \sqrt{e(k) + 0.5} \end{aligned} \tag{4.2}$$

where $\mathcal{F}$ denotes the Fourier transform operation, H_f represents the ideal single frequency pass filter. The constant 0.5 is added to account for the DC level of the signal that is lost due to the fact that the notch pass filter suppresses the DC component in the signal $|p(k)|$. The signal $e(k)$ is checked and corrected so that its amplitude does not cross 0.45 (or its range $\not> 0.9$) in order to keep the square root real.

The effects of the sinusoidal variation are now removed from $r0(k)$ and $r1(k)$ by applying $r0(k) = r0(k)/p_c(k)$ and $r1(k) = r1(k)/p_c(k)$ before continuing with further receiver functions. The filtering process is started only after all the frames

required to be stored are available. Data equivalent to 20 frames were chosen to be stored for this implementation to have at least 4 cycles of the sinusoid at 0.2 CPF.

The basic block diagram can now be rewritten as shown in Figure 4.2

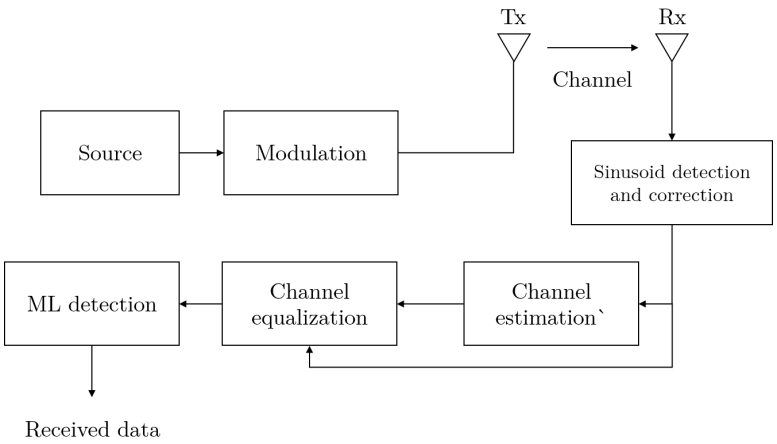

Figure 4.2. Revised block diagram with sinusoidal fading power variation cancellation system included

5. RESULTS

5.1. INTERMEDIATE RESULTS

The proposed method was implemented along with the previously explained simulation. Observations from the implemented method are presented here. Figure 5.1 shows the received signal that was collected over 20 frames of data.

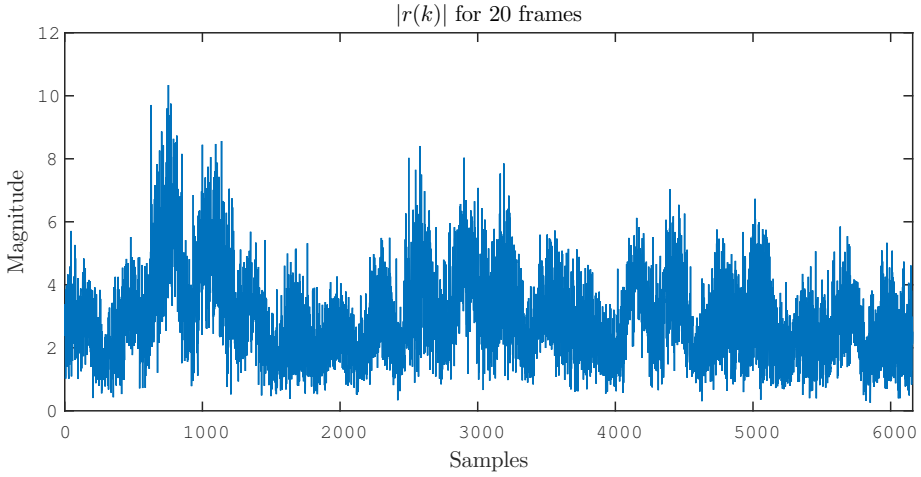

Figure 5.1. Received signal power over 20 frames of data

Figure 5.2 shows the extracted sinusoidal variation signal $e(k)$ over 20 frames of data where the 20^{th} frame corresponding to the current received frame. This consists of a sinusoidal disturbance of 80% variation at 3 cpf.

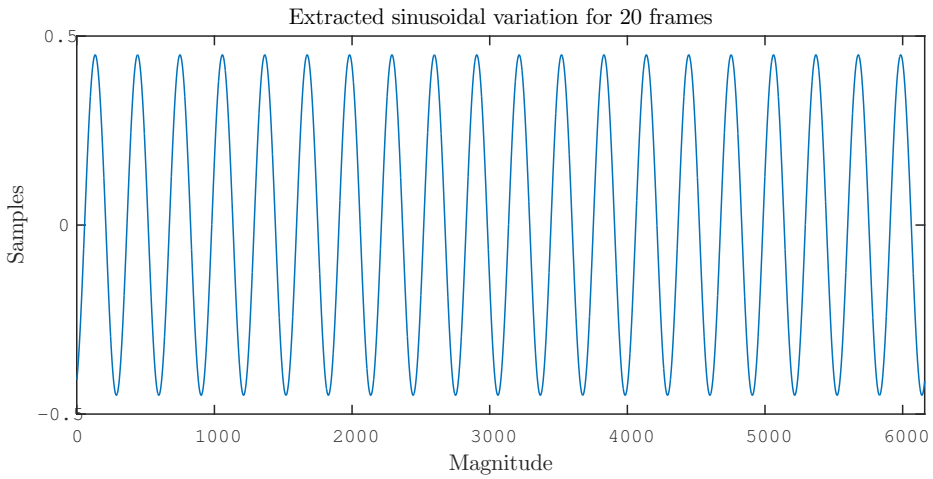

Figure 5.2. Extracted sinusoidal variation signal $e(k)$ for 20 frames

Figure 5.3 shows the conditioned signal $p_c(k)$ for the last data frame in comparison with the original sinusoidal variation used to modify the generated fading.

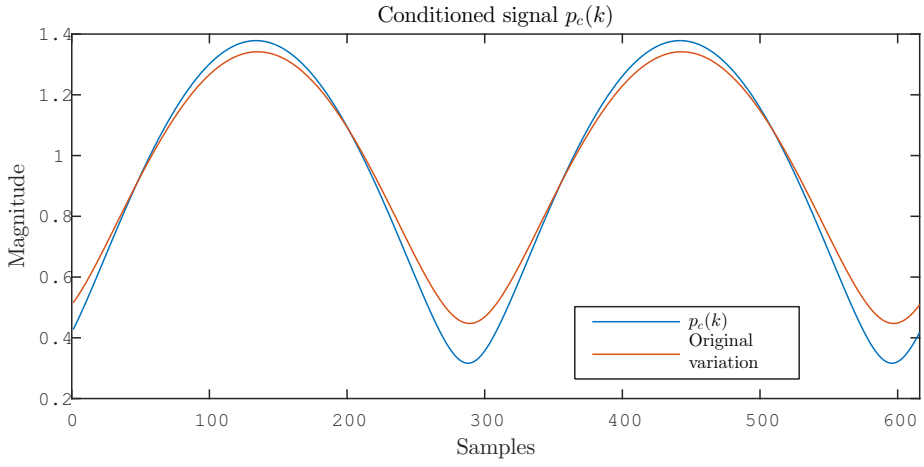

Figure 5.3. $p_c(k)$ and $\sqrt{a + C\cos\Theta}$ for comparision

Figure 5.4 shows the comparison between the received signal without cancellation of sinusoidal power variation and the same received signal after cancellation, both at receiver Rx_0s.

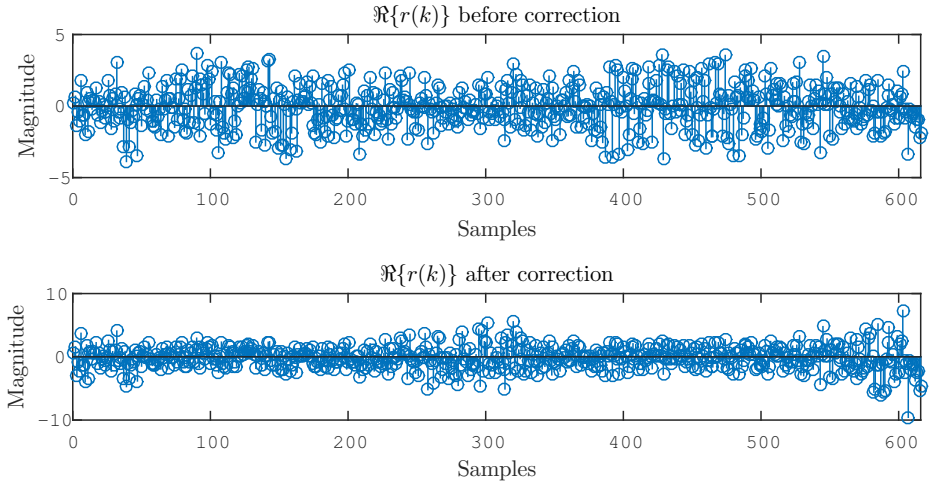

Figure 5.4. Values of $r(k)$ for current frame before cancellation and values of $r(k)$ for current frame after cancellation

Figure 5.5 shows the comparision between original fading envelopes with sinusoidal variation, original fading envelopes without sinusoidal variation and fading estimates calculated by the channel estimator using the proposed method is used.

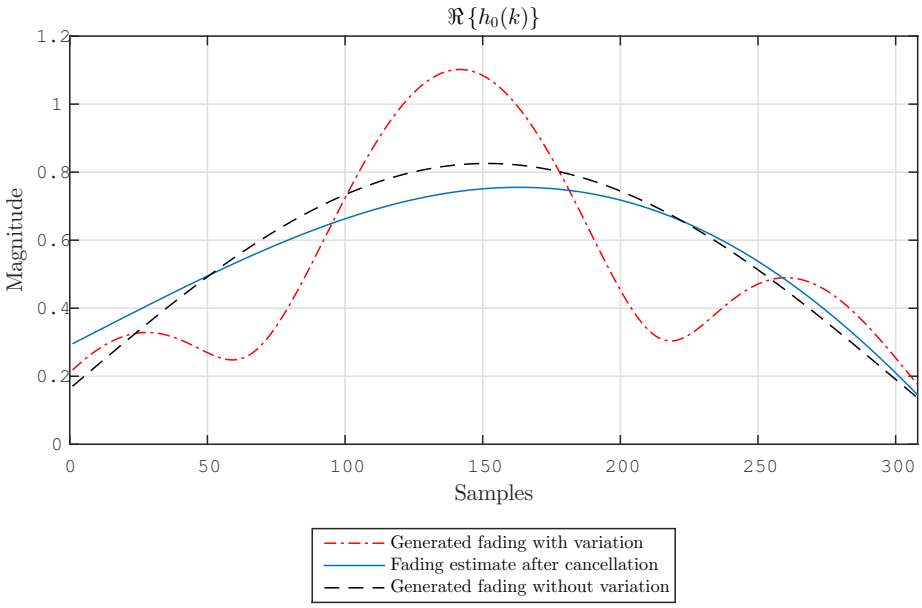

Figure 5.5. Original fading with sinusoidal variation, fading estimate after conditioning, and original fading without sinusoidal variation.

5.2. BER RESULTS

Figure 5.6 shows the following results (indicated by their line style used).

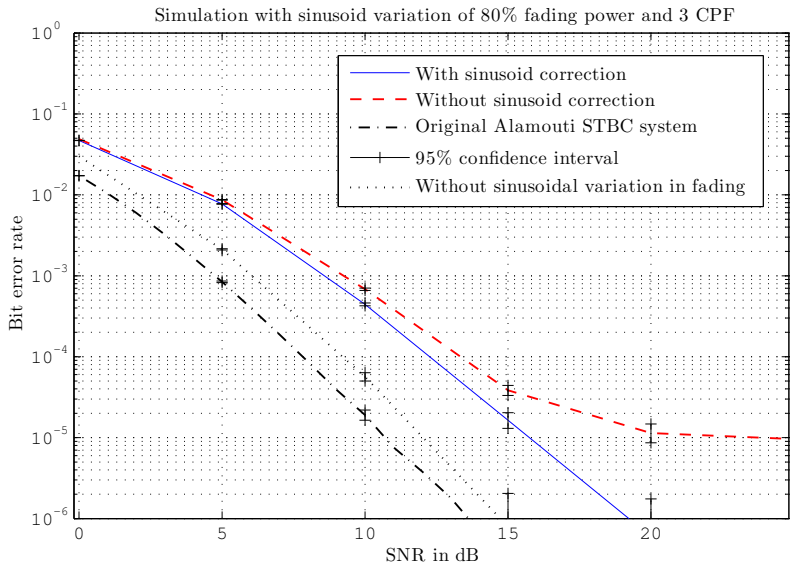

Figure 5.6. BER performance of the simulated system and proposed sinusoidal variation detection and correction scheme

- **Dash-dot:** This indicates the BER of the original Alamouti STBC wireless system that assumes 100% knowledge of channel coefficients.
- **Dotted:** This curve indicates the BER of the system in question, which has a mismatch between expected Doppler frequency and actual fading Doppler frequency.
- **Dashed:** This curve represents the BER of the current system when a sinusoidal variation is introduced in the fading with a variation of 80% in fading power and a frequency of 3 CPF.
- **Solid:** This shows the BER of the same system when a sinusoidal variation detection and correction scheme is employed.

Each BER value in Figure 5.6 is shown with a 95% confidence interval denoted by lines marked with a '+' sign. The BER of the simulated system was improved by more than 10 dB at an SNR of 20dB and at least 3dB at an SNR of 15dB.

6. CONCLUSION

A modular scheme to detect and correct sinusoidal variations in wireless fading channels is proposed for wireless communication systems based on slow fading and channel estimation. This scheme was effective in combating the performance reduction due to any sinusoidal variations in a wireless communication system, as discussed in results.

Furthermore, the proposed scheme can be modified to adapt to combating regular fading power variations of any kind, if the variations can be modeled as a sum of sinusoids, by making required adjustments to the frequency detection system. The proposed scheme can be modified to be used for modulation schemes other than PSK (like QAM modulation).

APPENDIX A-0.4IN

MAIN SIMULATION FILE : MAIN.M

```
% ALAMOUTI CODE 2 X 2 IMPLEMENTATION WITH
   ESTIMATION
%
   ********************************************************

% Sushruth Sastry
% MS&T ECE
%
   ********************************************************

% Disable next line if used as a function
clc;clear all;
close all;
set(0,'defaultaxesfontname','CMU Serif');   %
   styling the plots

%% Configuration

% Trained data
load 'data/pilots.mat';
load 'data/H.mat';

% change factors
sps = 4;                            % Average
   samples per symbol
snr = 0:2.5:25;      % SNR in dB
simcount = 5e5;      % Simulation end count in
   bits
M = 8;                              % Fading paths
perin = 80;                         % percent change
    in fading power
cpf = 0.1;                          % Sinusoidal
   variations per frame
reserve = 10;             % reserve number of
   frames

wdrange = 2;         % Vary doppler frequency by
   this amount in Hz
wdbase = 13;         % Set actual doppler
   frequency of fading


% Calculating the parameters
wdo = wd;
```

```
t1 = (0:blocksize-1)*Ts;
ttemp = t1;
frametime = blocksize*Ts;

errors = 0*snr;
count = 0;

pc = 0.5*perin/100;
a0(blocksize) = 0;
a1 = a0;
rx = a0;

% storage variables
rxstored = zeros(length(t1),reserve,2,length(snr
   ));
pchangestore = [];
phase = rand()*2*pi;

params = cell(1,4);
for i = 1:4
        params{i} = fadingparams(M);    % M path
            fading
end

reverseStr = '';
fprintf('
   ------------------------------------------------\
   n');
fprintf('Simulation of 2X2 MIMO system using
   Alamouti STBC \n');
fprintf('
   ------------------------------------------------\
   n');

%% Simulation
tic

fcount = 0;
N = numel(rxstored(:,:,1,1));
fs = 1/Ts;
step = fs/N;
f = 0:step:fs-step;

while (count < simcount-blocksize)
```

```
msg = sprintf('Progress: %d of %d bits
   processed. (%.2f %%%%)\n', ...
         count, simcount, (count/simcount
            )*100);
fprintf([reverseStr, msg]);
reverseStr = repmat(sprintf('\b'), 1,
   length(msg)-1);

% calculate power variation & doppler
   variation
vary = cos(2*pi*t1*cpf/frametime + phase
   );
pchange = vary*pc + 0.5;
wdo = 2*pi*((rand() - 0.5)*wdrange +
   wdbase);

%% Transmission

% Generating signal

s = (randi(2,[1 blocksize]) - 1.5)*2;

% Insert pilots

s(pilotpositions*2) = 1;
s(pilotpositions*2-1) = 1;

a0(1:2:blocksize) = s(1:2:end);
   % Antenna 0 data
a1(1:2:blocksize) = s(2:2:end);
   % Antenna 1 data
a0(2:2:blocksize) = -conj(s(2:2:end));
a1(2:2:blocksize) = conj(s(1:2:end));

% upsampling (timing error intended if '
   sps' is not an integer)
t = linspace(t1(1)-(0.5*Ts),t1(end)
   +(0.5*Ts),numel(t1)*sps);

signal0 = interp1(t1,a0,t,'nearest');
signal1 = interp1(t1,a1,t,'nearest');

% Adjusting for interpolation errors
signal0(1:ceil(sps/2)) = a0(1);
```

```
        signal0(end-ceil(sps/2):end) = a0(end);
        signal1(1:ceil(sps/2)) = a1(1);
        signal1(end-ceil(sps/2):end) = a1(end);

        % Generate Fading at wd/2 since
           framesize is doubled due to STBC

%       h0 = rfading( t1, M, 0.5, wdo/2, params
   {1});
%       h1 = rfading( t1, M, 0.5, wdo/2, params
   {2});
%       h2 = rfading( t1, M, 0.5, wdo/2, params
   {3});
%       h3 = rfading( t1, M, 0.5, wdo/2, params
   {4});

        h0 = rfading( t1, M, pchange(:), wdo/2,
           params{1});
        h1 = rfading( t1, M, pchange(:), wdo/2,
           params{2});
        h2 = rfading( t1, M, pchange(:), wdo/2,
           params{3});
        h3 = rfading( t1, M, pchange(:), wdo/2,
           params{4});

        % Original for reference
        h0r = h0(1:2:end).';
        h1r = h1(1:2:end).';
        h2r = h2(1:2:end).';
        h3r = h3(1:2:end).';

        h01 = interp1(t1,h0,t,'linear');
        h11 = interp1(t1,h1,t,'linear');
        h21 = interp1(t1,h2,t,'linear');
        h31 = interp1(t1,h3,t,'linear');

     % interpolation error adjust
        h01(1:ceil(sps/2)) = h0(1);
        h01(end-ceil(sps/2):end) = h0(end);
        h11(1:ceil(sps/2)) = h1(1);
        h11(end-ceil(sps/2):end) = h1(end);
        h21(1:ceil(sps/2)) = h2(1);
        h21(end-ceil(sps/2):end) = h2(end);
        h31(1:ceil(sps/2)) = h3(1);
```

```
h31(end-ceil(sps/2):end) = h3(end);

%% Reception

for i = 1:length(snr)
        % Corrupting the signal
        ra = awgn(signal0.*h01 + signal1
           .*h11,snr(i),'measured');
        rb = awgn(signal0.*h21 + signal1
           .*h31,snr(i),'measured');

        % Downsampling
        rta = interp1(t,ra,t1,'linear');
        rtb = interp1(t,rb,t1,'linear');

        % Detection and correction
           ======================

        rxstored(:,:,:,i) = circshift(
           rxstored(:,:,:,i),[0 -1 0]);

        rxstored(:,end,1,i) = rta;
        rxstored(:,end,2,i) = rtb;

        if(fcount >= reserve)
                [notch, dt] = findsine(
                   rxstored(:,:,:,i), 1/
                   Ts, 2*pi*10, 1);

                [~,findx] = min(abs(f-
                   notch(1)));
                fact = f(findx);
                idx = (f == fact) | (f
                   == fs-fact);

                sig = real(ifft(fft(abs(
                   dt(:))).*idx'));
    if(range(sig) > 0.9)
        sig = 0.9*sig/range(sig);
    end
                correction = real(sig(
                   end-blocksize+1:end))
                   + 0.5;
    correction = sqrt(2*correction);
```

```
if(sum(angle(correction)) > 0)
     error('Complex correction
        signal');
end

            rta = rta./correction';
            rtb = rtb./correction';
            return
    end

    % End detection and correction
       ==================

    % Extracting
    r0 = rta(1:2:end);
    r1 = rta(2:2:end);
    r2 = rtb(1:2:end);
    r3 = rtb(2:2:end);

    % Channel estimation
    uc0 = r0(pilotpositions);
    uc1 = r1(pilotpositions);
    uc2 = r2(pilotpositions);
    uc3 = r3(pilotpositions);

    h0c = (uc0-uc1)/2;
    h1c = (uc0+uc1)/2;
    h2c = (uc2-uc3)/2;
    h3c = (uc2+uc3)/2;

    h0s = (H*h0c.').';
    h1s = (H*h1c.').';
    h2s = (H*h2c.').';
    h3s = (H*h3c.').';

    % Reception

    s0c = conj(h0s).*r0+h1s.*conj(r1
       ) + conj(h2s).*r2+h3s.*conj(r3
       );
    s1c = conj(h1s).*r0-h0s.*conj(r1
       ) + conj(h3s).*r2-h2s.*conj(r3
       );
```

```
                rx(1:2:blocksize) = s0c;
                rx(2:2:blocksize) = s1c;

                rx(real(rx) >= 0) = 1;
                rx(real(rx) < 0) = -1;

                %% counting errors
                errors(i) = errors(i) + sum(rx~=
                   s);
        end

        t1 = t1 + frametime;
        count = count + blocksize;
        fcount = fcount + 1;
end
fprintf('\n
   ------------------------------------------\
   n');
fprintf('End of simulation. \n');
toc
fprintf('
   ------------------------------------------\
   n');

%% Results
figure;
semilogy(snr,errors/count);
hold on;
% semilogy(snr,errors/count1,'r');
confidenceplotter(snr,errors,repmat(count, [1
   length(snr)]));
legend('No periodic component','95% Confidence
   interval');
% confidenceplotter(snr,errors1,count1);
xlim([0 50]);
grid on;
xlabel('SNR in dB');
ylabel('Bit error rate');
ylim([1e-6 1]);
```

APPENDIX B-0.4IN

SUPPORTING FUNCTION : RFADING.M

RAYLEIGH FADING GENERATOR

```
function [ z ] = rfading( t, M, pow, wd, params, rayric )

%   Usage :
%
%       Z = RFADING(T, M, POW, WD, PARAMS);
%
%   Details :
%
%       Z               = rayleigh fading
%       T               = Time index
%       WD              = Doppler angular frequency (
   single or same size as t)
%       M               = Number of paths to consider (
   usually 8)
%       PARAMS  = a struct containing [1xM] arrays of
   alpha, psi and phi.
%       POW             = required overall fading power or
%                                 instantaneous power the
   same size as t.
zc = zeros(length(t),1);
zs = zc;

if(~exist('rayric','var'))
        rayric = false;
end

c = sqrt(1/M);

for i = 1:length(t)
        zc(i) = c*sum(cos(wd.*t(i)*cos(params{1}) + params
           {2}));
        zs(i) = c*sum(sin(wd.*t(i)*sin(params{1}) + params
           {2}));
end


if(rayric)
        po = (rand() - 0.5)*2*pi;
        zc = (zc.' + sqrt(pow(2,:)).*cos(wd.*t.*cos(pi/4)
           + po))./sqrt(1 + pow(2,:));
        zs = (zs.' + sqrt(pow(2,:)).*sin(wd.*t.*sin(pi/4)
```

```
            + po))./sqrt(1 + pow(2,:));
end

z = sqrt(pow(1,:)'*2).*(zc(:) + 1i*zs(:));

end
```

APPENDIX C-0.4IN

SUPPORTING FUNCTION : CONFIDENCEPLOTTER.M

CONFIDENCE INTERVAL PLOTTER

```
function [  ] = confidenceplotter( snr,errors,count)
%UNTITLED3 Summary of this function goes here
%   Detailed explanation goes here

[ber,interval] = berconfint(errors,count);
for i = 1:numel(snr)
    if(ber(i) > 0)
        semilogy([snr(i) snr(i)], interval(i,:),'k-+');
    end
end
end
```

APPENDIX D-0.4IN

SUPPORTING FUNCTION : FADINGPARAMS.M

FADING PARAMETER GENERATOR

```
function [ params ] = fadingparams(M)
%   FADINGPARAMS Summary of this function goes here
%   Detailed explanation goes here

theta = (rand(1)-0.5)*2*pi;
alpha = (2*pi*[1:M] - pi + theta)/(4*M);
phi = (rand(1,M)-0.5)*2*pi;
psi = (rand(1,M)-0.5)*2*pi;

params = {alpha,phi,psi};

end
```

APPENDIX E-0.4IN

SUPPORTING FUNCTION : FINDSINE.M

SINUSOIDAL VARIATION DETECTOR

```
function [ notch, d ] = findsine( rxstored, fs, wd, ~)
%FINDSINE Summary of this function goes here
%   Detailed explanation goes here

n = numel(rxstored(:,:,1));
d1 = abs(reshape(rxstored(:,:,1),1,n));
d2 = abs(reshape(rxstored(:,:,2),1,n));

d = (d1 + d2);

m = size(rxstored,1);
fn = (0:m-1)'/m;

% phase 1
f1 = 0;
f2 = wd;
w1 = exp(-1i*2*pi*(f2-f1)/(m*fs));
a1 = exp(1i*2*pi*f1/fs);
z = czt(abs(d)-mean(d),m,w1,a1);
fa = (f2-f1)*fn + f1;

% applying ramp to first phase
ramp = find(fa<wd);
ramp = ramp/max(ramp);
ramp = ramp.^(1/3);
z(fa<wd) = z(fa<wd).'.*ramp;

% phase 2
f1 = wd;
f2 = fs/2;
w = exp(-1i*2*pi*(f2-f1)/(m*fs));
a = exp(1i*2*pi*f1/fs);
z1 = czt(abs(d)-mean(d),m,w,a);
fb = (f2-f1)*fn + f1;

subplot(2,1,1)
plot(fa,abs(z)/max(abs(z)));
axis([fa(1) fa(end) 0 1]);

subplot(2,1,2)
plot(fb,abs(z1)/max(abs(z)));
```

```
axis([fb(1) fb(end) 0 1]);

mx1 = max(abs(z1));
z1(abs(z1) < 0.75*mx1) = 0;
[~,l] = findpeaks([0 abs(z1) 0]);
l = l - 1;

if(~isempty(l))
        if(numel(l) > 1)
                [~,i] = max(abs(z));
                z = czt(abs(d),m,w1,a1);
                [notch] = [fa(i) z(i)/m];
        else
                [notch] = [fb(l) z(l)/m];
        end
else
        [~,i] = max(abs(z));
        z = czt(abs(d),m,w1,a1);
        [notch] = [fa(i) z(i)/m];
end

end
```

APPENDIX F-0.4IN

SUPPORTING FUNCTION : COMBINER.M

STBC COMBINER

```
function [ h0s, h1s, h2s, h3s ] = combiner( rt, H ,
   pilotpositions, pe, pavg)
%[sc] = COMBINER(rt,h) - Alamouti combiner for 2 x 2
%
%---- Inputs -------------------------
% rt     = [rta(:) rtb(:)]
% h              = [h0s(:) h1s(:) h2s(:) h3s(:)]
%
%---- Outputs ------------------------
% rx     = rx

r0 = rt(1:2:end,1)./sqrt(pe/2).*sqrt(pavg/4);
r1 = rt(2:2:end,1)./sqrt(pe/2).*sqrt(pavg/4);
r2 = rt(1:2:end,2)./sqrt(pe/2).*sqrt(pavg/4);
r3 = rt(2:2:end,2)./sqrt(pe/2).*sqrt(pavg/4);

uc0 = r0(pilotpositions);
uc1 = r1(pilotpositions);
uc2 = r2(pilotpositions);
uc3 = r3(pilotpositions);

h0c = (uc0-uc1)/2;
h1c = (uc0+uc1)/2;
h2c = (uc2-uc3)/2;
h3c = (uc2+uc3)/2;

h0s = (H*h0c);
h1s = (H*h1c);
h2s = (H*h2c);
h3s = (H*h3c);
end
```

APPENDIX G-0.4IN

SUPPORTING FUNCTION : COMDIST.M

DISTANCE METRIC CALCULATOR FOR ML DEMODULATION

```
function [ out ] = comdist( x,y )

    out = (x - y).*(conj(x) - conj(y));

end
```

BIBLIOGRAPHY

[1] G. L. Stüber, *Principles of mobile communication*. Springer Science & Business Media, 2011.

[2] T. S. Rappaport *et al.*, *Wireless communications: principles and practice*, vol. 2. Prentice Hall PTR New Jersey, 1996.

[3] N. Jindal and A. Lozano, "Fading models and metrics for contemporary wireless systems," in *Signals, Systems and Computers (ASILOMAR), 2010 Conference Record of the Forty Fourth Asilomar Conference on*, pp. 625–629, Nov 2010.

[4] A. Alnoman and T. Ismaeel, "Detection of shadow fading in wireless networks," in *Future Communication Networks (ICFCN), 2012 International Conference on*, pp. 29–34, April 2012.

[5] B. L. Edington and T. A. Khan, "Method of source coding and harmonic cancellation for vibrational geophysical survey sources," Jan. 1 1991. US Patent 4,982,374.

[6] R. Marino, G. Santosuosso, and P. Tomei, "Robust adaptive compensation of biased sinusoidal disturbances with unknown frequency," *Automatica*, vol. 39, no. 10, pp. 1755 – 1761, 2003.

[7] M. Bodson and S. C. Douglas, "Adaptive algorithms for the rejection of sinusoidal disturbances with unknown frequency," *Automatica*, vol. 33, no. 12, pp. 2213–2221, 1997.

[8] J. Breithaupt, "Doppler system," Aug. 11 1964. US Patent 3,144,646.

[9] A. Kulkarni, "Performance analysis of zero forcing and minimum mean square error equalizers on multiple input multiple output system on a spinning vehicle," 2014.

[10] M. Cheffena, "Physical-statistical channel model for signal effect by moving human bodies," *EURASIP Journal on Wireless Communications and Networking*, vol. 2012, no. 1, pp. 1–13, 2012.

[11] D. Mizukami, K. Kodera, and H. Yasukawa, "Frequency offset compensation for ofdm receiver using rotating concyclic antenna," in *Circuits and Systems, 2008. ISCAS 2008. IEEE International Symposium on*, pp. 2478–2481, IEEE, 2008.

[12] R. Lyons, "Quadrature signals: Complex, but not complicated," *URL: http://www. dspguru. com/info/tutor/quadsig. htm*, 2000.

[13] Y. R. Zheng and C. Xiao, "Simulation models with correct statistical properties for rayleigh fading channels," *Communications, IEEE Transactions on*, vol. 51, no. 6, pp. 920–928, 2003.

[14] B. Sklar, "Rayleigh fading channels in mobile digital communication systems. i. characterization," *Communications Magazine, IEEE*, vol. 35, no. 7, pp. 90–100, 1997.

[15] C. Xiao and J. C. Olivier, "Nonselective Fading Channel Estimation with Nonuniformly Spaced Pilot Symbols," *International Journal of Wireless Information Networks*, vol. 7, pp. 177–185, July 2000.

[16] S. M. Alamouti, "A simple transmit diversity technique for wireless communications," *Selected Areas in Communications, IEEE Journal on*, vol. 16, no. 8, pp. 1451–1458, 1998.

[17] R. Wilson, "A note on the zeros of the bessel function," *Proceedings of the Edinburgh Mathematical Society (Series 2)*, vol. 6, no. 01, pp. 17–18, 1939.

[18] P. Stephen J. Ludwick, Ph.D. Joseph A. Profeta, "Harmonic cancellation algorithms enable precision motion control," *Motion System Design*, May 2011.

[19] L. J. Brown and Q. Zhang, "Periodic disturbance cancellation with uncertain frequency," *Automatica*, vol. 40, no. 4, pp. 631–637, 2004.

[20] M. Bodson, "Rejection of periodic disturbances of unknown and time-varying frequency," *International Journal of Adaptive Control and Signal Processing*, vol. 19, no. 2-3, pp. 67–88, 2005.

[21] M. Bodson, J. S. Jensen, and S. C. Douglas, "Active noise control for periodic disturbances," *Control Systems Technology, IEEE Transactions on*, vol. 9, no. 1, pp. 200–205, 2001.

[22] B. A. Francis and W. M. Wonham, "The internal model principle of control theory," *Automatica*, vol. 12, no. 5, pp. 457–465, 1976.

[23] P. De La Cuadra, A. Master, and C. Sapp, "Efficient pitch detection techniques for interactive music," in *Proceedings of the 2001 International Computer Music Conference*, pp. 403–406, 2001.

[24] R. O. Schmidt, "Multiple emitter location and signal parameter estimation," *Antennas and Propagation, IEEE Transactions on*, vol. 34, no. 3, pp. 276–280, 1986.

[25] R. Roy and T. Kailath, "Esprit-estimation of signal parameters via rotational invariance techniques," *Acoustics, Speech and Signal Processing, IEEE Transactions on*, vol. 37, no. 7, pp. 984–995, 1989.

[26] Mathworks, *Pseudospectrum using MUSIC algorithm.* Mathworks, 2015.

[27] O. Besson and P. Stoica, "Analysis of music and esprit frequency estimates for sinusoidal signals with lowpass envelopes," *Signal Processing, IEEE Transactions on*, vol. 44, pp. 2359–2364, Sep 1996.

[28] R. Narasimhan and D. C. Cox, "A generalized doppler power spectrum for wireless environments," *Communications Letters, IEEE*, vol. 3, no. 6, pp. 164–165, 1999.

[29] A. Anastasopoulos and K. M. Chugg, "An efficient method for simulation of frequency selective isotropic rayleigh fading," in *Vehicular Technology Conference, 1997, IEEE 47th*, vol. 3, pp. 2084–2088, IEEE, 1997.

[30] G. D. Martin, "Chirp z-transform spectral zoom optimization with matlab," *Sandia National Laboratories Report SAND2005-7084*, 2005.

VITA

Sushruth Sastry was born in Bangalore, India. After completing his schoolwork at Indian High School in Bangalore in 2006, Sushruth entered Yellamma Dasappa Institute of Technology affiliated to Visvesvaraya Technological University in Bangalore. He received a Bachelor of Engineering with a major in Electronics and Communication Engineering from Visvesvaraya Technological University in May 2012. During the following year, he was employed as a software engineer at Ezswype Business Solutions, Gurgaon, India. In December 2015, he Completed his MS degree from Electrical engineering department of Missouri University of Science and Technology at Rolla, MO, USA.